© 2017. Published by The Company of Biologists Ltd | Development (2017) 144, 2032-2044 doi:10.1242/dev.145920

RESEARCH ARTICLE

Regulation of neuromuscular junction organization by Rab2 and its effector ICA69 in *Drosophila*

Bhagaban Mallik[1], Manish Kumar Dwivedi[1], Zeeshan Mushtaq[1], Manisha Kumari[2], Praveen Kumar Verma[2] and Vimlesh Kumar[1,*]

ABSTRACT

The mechanisms underlying synaptic differentiation, which involves neuronal membrane and cytoskeletal remodeling, are not completely understood. We performed a targeted RNAi-mediated screen of *Drosophila* BAR-domain proteins and identified islet cell autoantigen 69 kDa (ICA69) as one of the key regulators of morphological differentiation of the larval neuromuscular junction (NMJ). We show that *Drosophila* ICA69 colocalizes with α-Spectrin at the NMJ. The conserved N-BAR domain of ICA69 deforms liposomes *in vitro*. Full-length ICA69 and the ICAC but not the N-BAR domain of ICA69 induce filopodia in cultured cells. Consistent with its cytoskeleton regulatory role, *ICA69* mutants show reduced α-Spectrin immunoreactivity at the larval NMJ. Manipulating levels of ICA69 or its interactor PICK1 alters the synaptic level of ionotropic glutamate receptors (iGluRs). Moreover, reducing PICK1 or Rab2 levels phenocopies *ICA69* mutation. Interestingly, Rab2 regulates not only synaptic iGluR but also ICA69 levels. Thus, our data suggest that: (1) ICA69 regulates NMJ organization through a pathway that involves PICK1 and Rab2, and (2) Rab2 functions genetically upstream of ICA69 and regulates NMJ organization and targeting/retention of iGluRs by regulating ICA69 levels.

KEY WORDS: Neuromuscular junction, ICA69, BAR domain, α-Spectrin, Rab2, Glutamate receptors

INTRODUCTION

Establishment of proper synaptic connections during animal development is essential for normal synaptic communication and is crucial for the behavioral output of an organism. These developmental processes involve morphological differentiation of neurons into highly specialized pre- and postsynaptic compartments for neurotransmitter release and its reception (Harris and Littleton, 2015; Shen and Scheiffele, 2010). During neuromorphogenesis, these events involve dynamic changes in the neuronal membrane as well as structural changes in the underlying neuronal cytoskeleton (Gallo, 2013; Nelson et al., 2013). Several biochemical and genetic studies have illustrated the role of membrane binding/bending and signaling proteins in neuromorphogenesis, both during neuronal differentiation and in mediating synaptic plasticity (Aspenström, 2014; Govek et al., 2004; Guerrier et al., 2009; Kessels and Qualmann, 2015; Murakoshi et al., 2011; Nahm et al., 2010).

[1]Department of Biological Sciences, AB-3, Indian Institute of Science Education and Research, Bhauri, Bhopal, Madhya Pradesh 462066, India. [2]National Institute of Plant Genome Research (NIPGR), New Delhi 110067, India.

*Author for correspondence (vimlesh@iiserb.ac.in)

Z.M., 0000-0003-3416-2289; V.K., 0000-0003-2206-4905

Received 20 October 2016; Accepted 19 April 2017

Bin-Amphiphysin-Rvs (BAR) domain-containing proteins with their membrane-deforming properties have recently emerged as key players in establishing neuronal morphology (Frost et al., 2008, 2009; Itoh et al., 2005; Kessels and Qualmann, 2015; Rao et al., 2010; Ukken et al., 2016). Studies in *Drosophila* have also implicated a role of BAR-domain proteins in regulating neuromuscular junction (NMJ) morphology (Chang et al., 2013; Coyle et al., 2004; Rikhy et al., 2002). Structural and bioinformatics analyses of several BAR-domain proteins have revealed that, in addition to a BAR module, many of these proteins have motifs that can regulate cytoskeleton and neuronal signaling (Aspenström, 2014; Coyle et al., 2004; Habermann, 2004; Kessels and Qualmann, 2015; Liu et al., 2015). Functional analysis of various BAR-domain proteins in cultured neuronal cells and genetic models are consistent with their role in modulating different aspects of cytoskeletal dynamics and neuronal signaling (Coyle et al., 2004; Dharmalingam et al., 2009; Rodal et al., 2008; Stanishneva-Konovalova et al., 2016). Moreover, proteins such as Syndapin and Nervous wreck (Nwk) can integrate membrane curvature generation with actin cytoskeletal dynamics in both neuronal and non-neuronal cells (Coyle et al., 2004; Dharmalingam et al., 2009; Kessels and Qualmann, 2006; Qualmann and Kelly, 2000). Similarly, some of the mammalian BAR-domain proteins, for instance RICH1 (also known as ARHGAP17) and oligophrenin 1, contain signaling modules that can directly interact with a variety of small GTPases (Houy et al., 2015; Kessels and Qualmann, 2015; Nadif Kasri et al., 2009; Nahm et al., 2010). Although existing structural, cell biological and biochemical analyses of the BAR-domain protein family elegantly bring out its crucial role in mediating various cellular functions, the *in vivo* context(s) in which these proteins function and mediate neuronal differentiation remains incompletely understood.

In order to gain deeper insights specifically in the context of neuronal development and function mediated by BAR domain-containing proteins, we carried out a targeted RNAi-mediated genetic screen and identified islet cell autoantigen 69 kDa (ICA69) as one of the key regulators of the *Drosophila* NMJ morphology. ICA69 is evolutionarily conserved from insects to mammals, and its function has been implicated in diabetes (Pietropaolo et al., 1993), neuroendocrine secretion (Pilon et al., 2000), dense core vesicle maturation (Sumakovic et al., 2009), acrosome formation (He et al., 2015) and synaptic targeting of AMPA receptors (Cao et al., 2007). Here, we show for the first time that ICA69 is one of the key regulators of *Drosophila* larval NMJ morphology and is crucial for targeting ionotropic glutamate receptor (iGluR) clusters at the NMJ. We propose a model in which Rab2 and the ICA69-PICK1 complex function in the same genetic pathway to regulate *Drosophila* NMJ organization.

RESULTS

Drosophila ICA69 promotes NMJ expansion

We performed a small-scale targeted RNAi-mediated genetic screen to identify BAR-domain proteins that affect NMJ morphology in

Development (2017) 144, 2032-2044 doi:10.1242/dev.145920

Drosophila. This screen identified ICA69 as one of the regulators of NMJ morphology; ubiquitous knockdown of *ICA69* resulted in a synaptic undergrowth phenotype (Table S1; Fig. 1).

We identified two transposon-tagged lines, *GS14708* and *GS13474*, that disrupt the *ICA69* gene (Fig. 1A). Both P-element insertion lines are homozygous lethal and die at the early third instar stage. Surprisingly, we found that hemizygous *GS14708/Df(3L)BSC553* or *GS13474/Df(3L)BSC553* were viable, suggesting that both of the P-element insertion lines have lethal background mutations. We next performed semi-quantitative RT-PCR to assess whether knockdown of *ICA69* or hemizygous *GS13474/Df(3L)BSC553* results in reduction of *ICA69* transcript level. Whereas the transcript level of *ICA69* was dramatically reduced in *Actin 5C*-Gal4-driven *ICA69* RNAi and *GS13474/Df(3L)BSC553*, the expression of a neighboring gene, *knockout* (*ko*), was unaltered (Fig. 1B). To confirm this result, we performed quantitative RT-PCR and found that whereas *Actin 5C*-Gal4-driven *ICA69* RNAi showed ∼55% reduction, the hemizygous mutant showed ∼35% reduction in *ICA69* transcript levels (Fig. S1A,B). As there was a specific reduction of the *ICA69* transcript, we performed all further experiments with hemizygous combination of *GS13474* and *Df(3L)BSC553*.

In order to quantify the NMJ growth phenotypes in *Actin 5C*-Gal4-driven *ICA69* RNAi, we measured the NMJ length, bouton number, bouton area and branch number in third instar larval NMJ synapses at muscle 6/7 of the A2 hemisegment. We found that, compared with the control synapses, *ICA69* knockdown resulted in

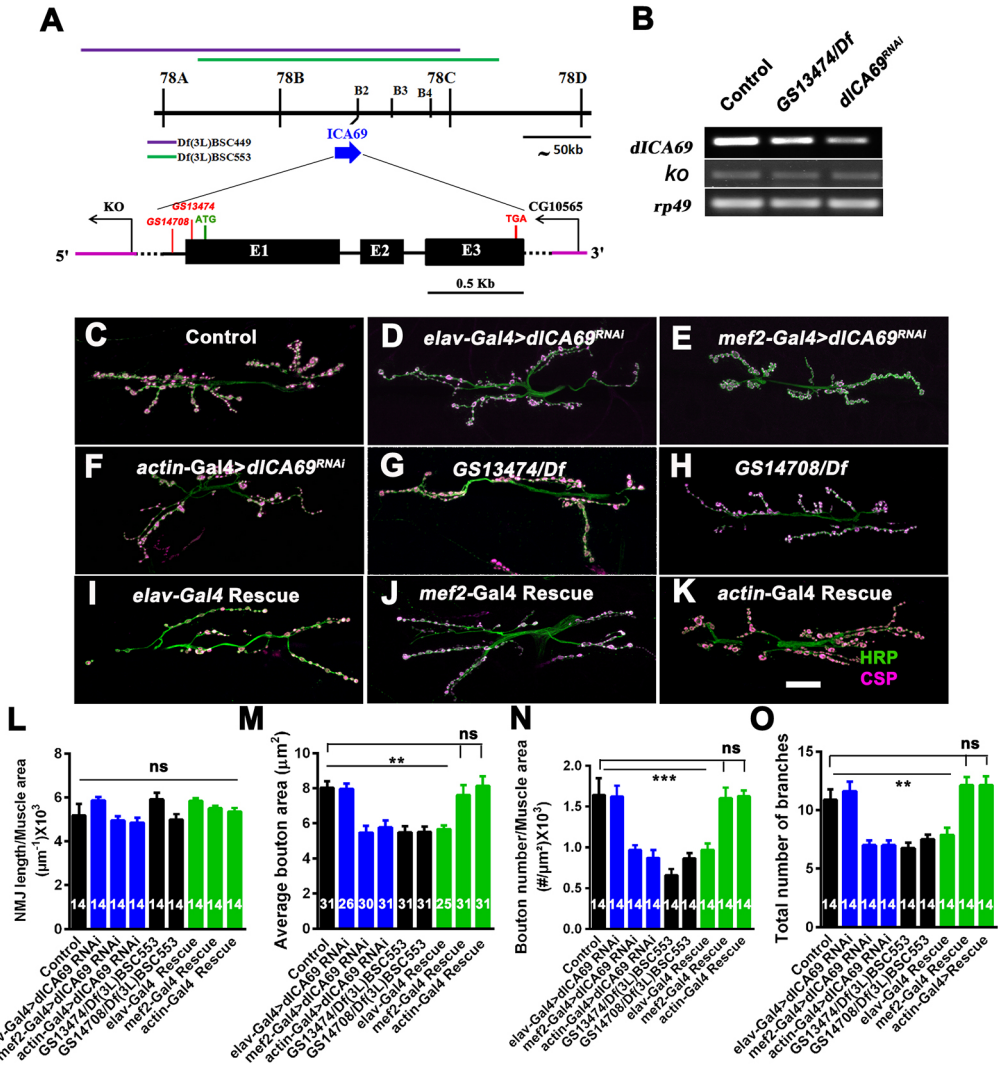

Fig. 1. Mutation in *ICA69* alters NMJ morphology in *Drosophila*. (A) Genomic organization of the *ICA69* locus showing exons (solid black boxes, E1-E3) and introns (thin lines). The insertion sites of two P-elements, *GS14708* and *GS13474*, are shown. Two of the deficiency lines, *Df(3L)BSC449* and *Df(3L)BSC553*, uncovering the *ICA69* locus are shown as purple and green lines, respectively. (B) Semi-quantitative RT-PCR showing transcript levels of *ICA69* in controls, hemizygous *GS13474*/*Df(3L)BSC553* and *Actin 5C*-Gal4-driven *ICA69* RNAi lines. The transcript level of the *ko* gene in *ICA69* mutants or *Actin 5C*-Gal4-driven *ICA69* RNAi flies is comparable to control levels. *rp49* transcript level was used as an internal RNA control. (C-K) Confocal images of NMJ synapses at muscle 6/7 of control (C), *elav*^{C155}-Gal4-driven *ICA69* RNAi (D), *mef2*-Gal4-driven *ICA69* RNAi (E), *Actin 5C*-Gal4-driven *ICA69* RNAi (F), *GS13474*/*Df(3L)BSC553* (G) and *GS14708*/*Df(3L)BSC553* (H) flies, and transgene-rescued animals *elav* ^{C155}*-Gal4/+;UAS-ICA69*^{FL}*/+;Df(3L)BSC553/GS13474* (I), *UAS-ICA69*^{FL}*/+;mef2-Gal4,Df(3L)BSC553/GS13474* (J) and *UAS-ICA69*^{FL}*/+;Actin 5C-Gal4,Df(3L)BSC553/GS13474* (K) double immunolabeled with CSP (magenta) and HRP (green). The NMJ morphological defect was rescued by expressing *ICA69* transgene in muscles but not neurons. Scale bar: 20 µm. (L-O) Histograms showing average NMJ length, bouton area, number of boutons and total number of branches per NMJ at muscle 6/7 of A2 hemisegments in the indicated genotypes. ***P*<0.001, ****P*<0.0001; ns, not significant. Error bars represent mean±s.e.m. Statistical analysis based on one-way ANOVA with post-hoc Tukey's test for multiple comparisons.

Development (2017) 144, 2032-2044 doi:10.1242/dev.145920

a significant reduction in the number of boutons per unit muscle area, bouton area and the total number of branches per muscle. Consistent with this observation, hemizygous combination of *ICA69* resulted in significantly reduced bouton number per unit muscle area as well as smaller NMJs (Fig. 1; Table S3). The bouton numbers and the synaptic undergrowth phenotypes were fully restored by expressing an *ICA69* transgene either in the muscles (*UAS-dICA69^{FL}/+; mef2-Gal4, Df(3L)BSC553/GS13474*) or ubiquitously in hemizygous animals (*UAS-dICA69^{FL}/+; Actin 5C-Gal4, Df(3L)BSC553/GS13474*) (Fig. 1; Table S3). These phenotypes could not be restored by expressing the *ICA69* transgene in neurons using pan-neuronal *elav*-Gal4 (*elav-Gal4/+; UAS-dICA69^{FL}/+; Df(3L)BSC553/GS13474*) (Fig. 1; Table S3). Taken together, these data suggest that ICA69 positively regulates NMJ expansion in *Drosophila* and has specific roles in the muscles to regulate NMJ morphology.

Drosophila ICA69 predominantly localizes with α-Spectrin at the NMJ

In order to gain further insights into ICA69 functions, we first generated polyclonal antisera against the N-terminal 361 amino acids of ICA69. Western blot analysis using this antibody revealed a single protein band of about 60 kDa in larval lysates (Fig. S1C). We next assessed the specificity of the anti-ICA69 antibody towards the endogenous protein. Immunocytochemistry of *Actin 5C*-Gal4-driven *ICA69* RNAi or hemizygous *ICA69* mutant larval NMJs revealed a significant decrease in ICA69 immunoreactivity. Moreover, ubiquitous overexpression of an *ICA69* transgene showed elevated ICA69 immunoreactivity at the larval NMJ (Fig. 2A,B). Consistent with this, western blot analysis revealed ∼50% reduction of ICA69 in *Actin 5C*-Gal4-driven *ICA69* RNAi or hemizygous *ICA69* mutant NMJs (Fig. 2C). Taken together, these data indicate that the anti-ICA69 antibody specifically recognizes endogenous ICA69 protein and that knockdown of *ICA69* as well as the hemizygous mutant show reduced ICA69 protein.

Although ICA69 is not enriched at mammalian synapses (Cao et al., 2007), we found that *Drosophila* ICA69 strongly localizes to the NMJ (Fig. 2D-F). *Drosophila* ICA69 perfectly colocalized with α-Spectrin, a major component of the postsynaptic cytoskeletal scaffold (Fig. 2G,H). At axons, ICA69 localizes with horseradish peroxidase (HRP), suggesting neuronal expression, but is not detectable within the boutons (Fig. 2D-F,I). Overexpressing an ICA69 transgene in motor neurons did not cause enrichment of ICA69 at the motor terminals (data not shown) suggesting that ICA69 is not normally trafficked to the presynapse. Taken together, these data suggest that *Drosophila* ICA69 surrounds the subsynaptic reticulum (SSR) and possibly regulates Spectrin cytoskeleton at the NMJ.

A postsynaptic submembrane Actin-Spectrin network functions as an organizing scaffold for pre- and postsynaptic assembly during postembryonic development (Pielage et al., 2006). Because ICA69 strongly colocalizes with α-Spectrin and mutation in *ICA69* altered NMJ morphology, we next investigated whether *ICA69* mutation alters Spectrin levels at the NMJ. Immunocytochemistry revealed that larvae with reduced ICA69 levels show significantly reduced α-Spectrin immunoreactivity (control, 100±8.2; *Actin 5C*-Gal4>*dICA69* RNAi, 69.1±4.7; *GS13474/Df(3L)BSC553*, 68.5±5.2) (Fig. 2J-M). Synaptic levels and distribution of other postsynaptic proteins, such as Dlg or Syndapin, were normal in the *ICA69* mutant (Fig. S2). Moreover, pre- or post-synaptic knockdown of ICA69 does not alter the synapse stability (Fig. S3). Normalizing levels of ICA69 ubiquitously by expressing an *ICA69* transgene restored the synaptic α-Spectrin level (93.3±6.2) (Fig. 2N). Taken together, these data indicate that ICA69 is involved in NMJ development, possibly by regulating the postsynaptic Spectrin cytoskeleton.

ICA69 deforms synthetic liposomes *in vitro* and generates filopodia in S2R+ cells

Drosophila ICA69, like its mammalian ortholog, consists of an N-BAR and an ICAC domain (Fig. 3A). The BAR domain binds and deforms phospholipids to generate membrane tubules and/or vesicles (Fricke et al., 2009; Masuda et al., 2006). Because ICA69 contains a BAR module, we first assessed whether the ability of this domain to deform synthetic liposomes is biochemically conserved. We found that the N-BAR domain (aa 1-234) of ICA69 deformed liposomes and induced tubular membrane structures within 10 min of incubation with liposomes. However, we predominantly observed membrane vesicles within 30 min of incubation with liposomes (Fig. 3B-D). This indicates that, like other N-BAR domain proteins, ICA69 N-BAR can deform synthetic membranes *in vitro* to generate tubules and vesicles.

Surprisingly, in cultured S2R+ cells, ICA69$^{N\text{-}BAR}$ did not induce any detectable tubules but rather gets targeted to the perinuclear region and forms structures that have a vesicle-like appearance (Fig. 3G,G′). Moreover, like endogenous ICA69 in S2R+ cells, these vesicular structures did not colocalize with established markers for Golgi bodies or endoplasmic reticulum (Fig. S4). Interestingly, expression of either full-length ICA69 (ICA69^{FL}) or the ICA69 ICAC domain (ICA69^{ICAC}) resulted in a massive induction of filopodia in S2R+ cells (untransfected, 1.1±0.2; transfection control, 1.08±0.2; N-BAR, 2.6±0.6; ICAC, 48.1±4.9; FL 31.1±3.7), where actin was strongly localized (Fig. 3E-J). Further analyses revealed that the filopodia induced by ICA69^{FL} or ICA69^{ICAC} show enrichment of SCAR and Wasp, two of the positive regulators of actin polymerization (Fig. 3K-P). We performed co-immunoprecipitation experiments to assess whether ICA69 directly interacts with SCAR and Wasp. However, we could not detect a direct binding between ICA69 and Wasp or SCAR (Fig. S5). This suggests that the ICAC domain of ICA69 can relocalize Wasp and SCAR at the site of filopodia, possibly through indirect interaction with the actin regulators; and that the N-BAR domain of ICA69 negatively influences the ICAC domain during filopodia formation.

Synaptic levels of iGluR subunits are tightly regulated by the endogenous ICA69 level

Because reduction of ICA69 in *Drosophila* leads to NMJ structural defects, we assessed experimentally whether it has a direct effect on synaptic transmission. Surprisingly, we did not find any significant change in any of the electrophysiological parameters such as spontaneous (miniature excitatory junction potentials, mEJPs) or evoked (excitatory junction potentials, EJPs) responses when compared with control animals. The quantal content was also not significantly altered in *ICA69* mutants (Fig. S6). These data reveal that, despite striking alteration in NMJ morphology, *ICA69* mutant synapses function normally.

Like most mammalian central excitatory synapses, iGluRs are the major components of *Drosophila* NMJs that elicit a response in the postsynapse (DiAntonio, 2006; Marrus and DiAntonio, 2004; Marrus et al., 2004). The iGluR family consists of two classes of tetrameric ionotropic glutamate receptor clusters – those containing GluRIIA and others containing GluRIIB. Glutamate receptor subunits GluRIII (GluRIIC), GluRIID and GluRIIE are invariant in the iGluR clusters (Marrus and DiAntonio, 2004; Qin et al., 2005). Because ICA69 negatively regulates AMPA receptor

Development (2017) 144, 2032-2044 doi:10.1242/dev.145920

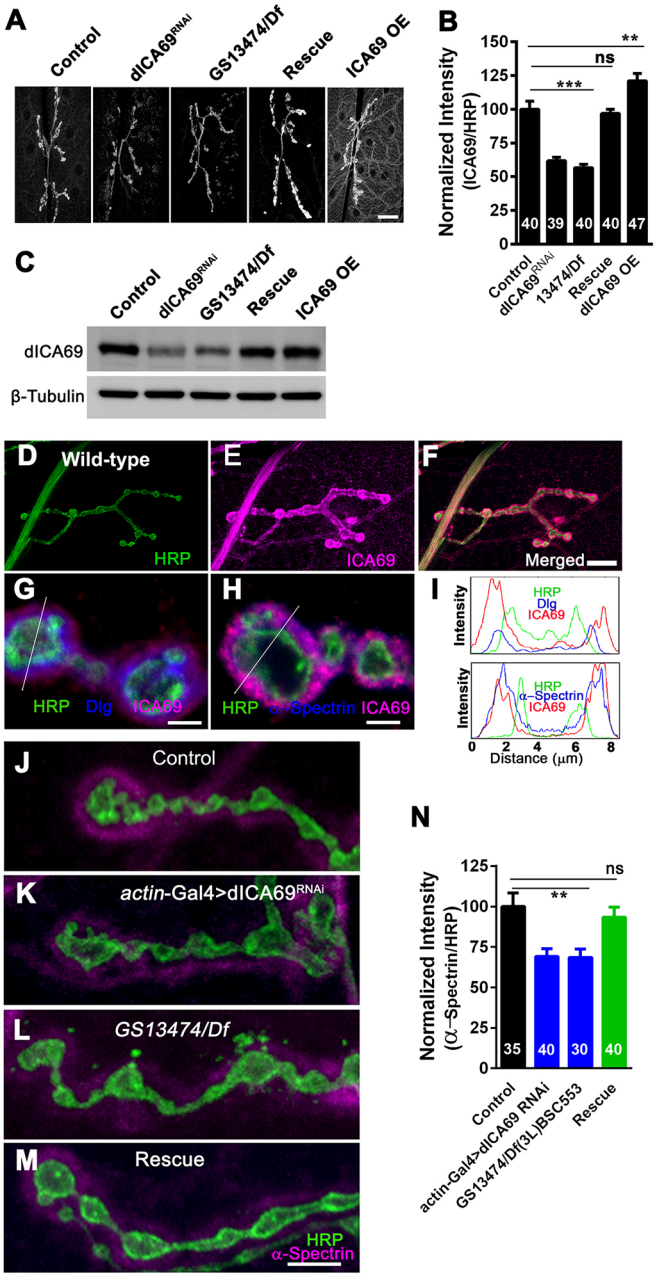

Fig. 2. *Drosophila* ICA69 predominantly localizes with Spectrin and correlates with its synaptic level at the larval NMJ. (A) Confocal images of third instar larval NMJ synapses in control, *Actin 5C*-Gal4-driven *ICA69* RNAi, hemizygous *ICA69* mutant, rescue [*UAS-ICA69^{FL}/+;Actin 5C-Gal4,Df(3L) BSC553/GS13474*] and *Actin 5C*-Gal4-driven ICA69 overexpressing (OE) animals, labeled with ICA69 antibody. (B) Histogram showing average ICA69 fluorescence at the NMJ of the indicated genotypes. (C) Western blot comparison of ICA69 protein in the muscles of the indicated genotypes. β-Tubulin was used as a loading control. (D-F) Confocal images of wild-type larval NMJ synapses at muscle 4 co-labeled with HRP (green) and ICA69 (magenta). Scale bar: 25 µm. (G,H) Single confocal section of boutons in third instar larval NMJs triple labeled with ICA69 (magenta), HRP (green) and Dlg (blue) (G) or ICA69 (magenta), HRP (green) and α-Spectrin (blue) (H). Note that ICA69 immunoreactivity strongly colocalizes with α-Spectrin. Scale bars: 2 µm. (I) Intensity plot profile for each antibody across the bouton (shown in G and H as thin line). Note that the ICA69 intensity profile closely matches that of the α-Spectrin intensity profile. (J-M) Confocal images of third instar larval NMJs in control, *Actin 5C*-Gal4-driven *ICA69* RNAi, *GS13474/Df(3L)BSC553* and ICA69 transgene-rescued [*UAS-dICA69^{FL}/+; Actin 5C-Gal4, Df(3L) BSC553/GS13474*] synapses, immunostained with anti-HRP (green) and α-Spectrin (magenta) antibodies. Scale bar: 10 µm. (N) Histogram showing synaptic levels of α-Spectrin in the indicated genotypes. Compared with controls (100±8.29), *Actin 5C*-Gal4-driven *ICA69* RNAi (69.10±4.78) or hemizygous *ICA69* mutant [*GS13474/Df(3L)BSC553*; 68.54±5.27] NMJs show a significant reduction in synaptic α-Spectrin level that is rescued by ubiquitously overexpressing a full-length ICA69 transgene. ***P*<0.001, ****P*<0.0001; ns, not significant. Error bars represent mean±s.e.m. Statistical analysis based on one-way ANOVA with post-hoc Tukey's test for multiple comparisons.

targeting and clustering in mammalian neurons (Cao et al., 2007), we next investigated whether any of the glutamate receptors at the fly NMJ were upregulated in *ICA69* mutant. Contrary to our expectations, we found that hemizygous *ICA69* mutant or *Actin 5C*-Gal4-driven *ICA69* RNAi flies showed a reduction of ∼40% for all three iGluR subunits analyzed (GluRIII, GluRIIA and GluRIIB) (Fig. 4; Table S4). The synaptic levels of glutamate receptors were restored in hemizygous *ICA69* mutant when an *ICA69* transgene was expressed in muscles or ubiquitously, but not in neurons (Fig. 4; Table S4). These data suggest that ICA69 functions in muscles to regulate synaptic targeting/retention of both GluRIIA- and GluRIIB-containing glutamate receptor clusters at the NMJ.

Overexpression of ICA69 in mammalian neurons alters synaptic AMPA receptor levels (Cao et al., 2007). Consistent with previous observations in mammalian neurons, overexpression of ICA69 in muscles dramatically reduced synaptic targeting of GluRIII, GluRIIA and GluRIIB (Fig. 4; Table S4). These observations suggest that endogenous stoichiometry of ICA69 with its other interacting partners is crucial for synaptic targeting/retention of various glutamate receptors at the *Drosophila* NMJ.

PICK1 regulates synaptic iGluR and ICA69 levels at the *Drosophila* NMJ

Expression of ICA69 and PICK1 is interdependent in adult *Drosophila* brain as well as in endocrine cell lines (Cao et al., 2013). PICK1 was not detectable at the NMJ synapses in *Drosophila* (Jansen et al., 2009). As our data conclusively demonstrates strong postsynaptic localization of ICA69, we next investigated whether RNAi-mediated knockdown of its binding partner PICK1 in muscle affects iGluR targeting at the NMJ. Surprisingly, we observed a dramatic reduction in synaptic levels of GluRIII (control, 100.0±3.8; *PICK1* RNAi, 76.1±2.4), GluRIIB (control, 100.0±3.1; *PICK1* RNAi, 66.1±2.9) and GluRIIA (control, 100.0±4.2; *PICK1* RNAi, 51.06±2.5) in animals with reduced PICK1 levels (Fig. 5A-G). Similar results were obtained with *Actin 5C*-Gal4-driven *PICK1* RNAi (Fig. 5H-J). Moreover, consistent with previous observations in *Drosophila* brain (Cao et al., 2013), we found significant reduction in ICA69 levels at *Drosophila* NMJs in *mef2*-Gal4-driven *PICK1* RNAi animals (control, 100.0±3.9; *PICK1* RNAi, 72.1±5.3) (Fig. 5K-M). Knockdown of *PICK1* using *Actin 5C*-Gal4 resulted in similar reduction of ICA69 level (Fig. 5N). These data suggest that although PICK1 is not enriched at the *Drosophila* NMJ, it still binds to and stabilizes ICA69 in muscles and regulates its synaptic levels.

RNAi-mediated knockdown of PICK1 or Rab2 phenocopies NMJ structural defects of *ICA69* mutation

Rab2, a member of the small GTPase family, has been shown to interact biochemically with mammalian ICA69 (Buffa et al., 2008). Our previous data suggest that PICK1 regulates ICA69 at the

Development (2017) 144, 2032-2044 doi:10.1242/dev.145920

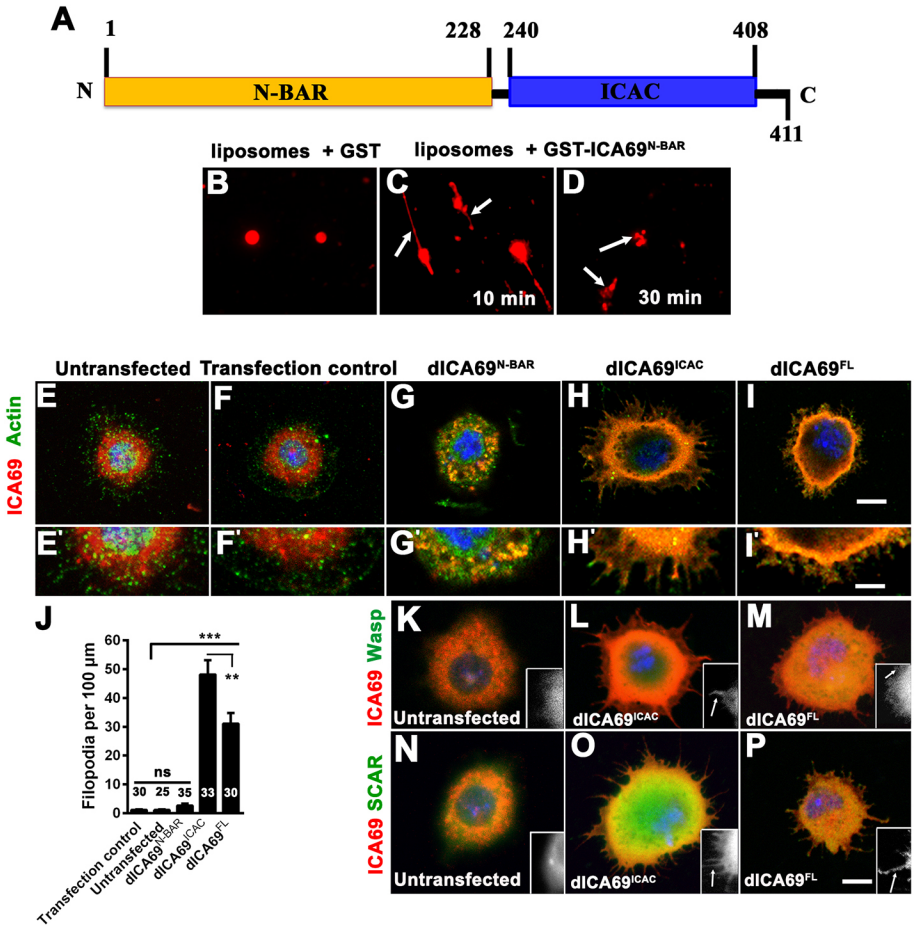

Fig. 3. ICA69 deforms synthetic liposomes *in vitro* and induces filopodia in cultured S2R+ cells. (A) Schematic of the domain organization of ICA69 showing the conserved N-terminal N-BAR domain and a C-terminal ICAC domain. (B-D) Synthetic liposomes containing rhodamine-conjugated phosphatidylethanolamine (PE) incubated with either GST or GST-ICA69-N-BAR domain and imaged by fluorescence microscopy. The N-BAR domain of ICA69 initially tubulates liposomes and then induces fission to generate vesicles. Arrows in D indicate vesicles generated by ICA69-N-BAR within 30 min of incubation with liposomes. Arrows in C indicate tubules generated by ICA69-N-BAR within 10 min of incubation with liposomes. (E-I′) Confocal images of untransfected S2R+ cells (E,E′) or S2R+ cells incubated with transfection reagent (Mirus *TransIT*; F,F′) ICA69$^{N\text{-}BAR}$ (aa 1-234; G,G′), ICA69^{ICAC} (aa 235-411; H,H′) or ICA69^{FL} (aa 1-411; I,I′) co-labeled with actin and ICA69 antibodies. Scale bar: 10 µm (E-I,K-P); 4 µm (E′-I′). (J) Histogram showing quantification of average number of filopodia per 100 µm in untransfected or various ICA69 domain-transfected S2R+ cells. ***P*<0.001, ****P*<0.0001; ns, not significant. Error bars represent mean±s.e.m. Statistical analysis based on one-way ANOVA with post-hoc Tukey's test for multiple comparisons. (K-M) Images of untransfected S2R+ cells (K) or cells transfected with either ICA69^{ICAC} (L) or full-length ICA69 (M) and immunolabeled with Wasp (green) and ICA69 (red) antibodies. Images in the inset represent Wasp immunofluorescence (shown by arrows) within the filopodia. (N-P) Images of untransfected S2R+ cells (N) or cells transfected with either ICA69^{ICAC} (O) or full-length ICA69 (P) and immunolabeled with SCAR (green) and ICA69 (red) antibodies. Images in the inset represent SCAR immunofluorescence (shown by arrows) within the filopodia. Note that SCAR is highly enriched at the tip of the filopodia.

Drosophila NMJ. Therefore, to determine whether PICK1 and Rab2 regulate NMJ development in a manner similar to ICA69, we ubiquitously knocked them down and analyzed the NMJ morphology. Interestingly, we found that reducing levels of PICK1 or Rab2 phenocopies *ICA69* NMJ structural defects (Fig. 6A-G). PICK1 or Rab2 reduction leads to smaller synapse size and reduced number of boutons per unit muscle area at the NMJ (control, 1.70±0.1; *mef2*-Gal4>*dRab2* RNAi, 0.95±0.1; *mef2*-Gal4>*dPICK1* RNAi, 0.97±0.12; *Actin 5C*-Gal4>*dRab2* RNAi, 0.94±0.17; *Actin 5C*-Gal4>*dPICK1* RNAi, 0.94±0.12) (Fig. 6H).

Because Rab2 and ICA69 loss-of-function mutants were not available, we assessed genetic interactions under hypomorphic conditions using RNAi against Rab2 and ICA69. We co-expressed *Rab2* and *ICA69* RNAi with 2X *Actin 5C*-Gal4 (*Actin 5C*-Gal4/+; UAS-*Rab2* RNAi/*Actin 5C*-Gal4, UAS-*dICA69* RNAi) or *PICK1* and *ICA69* RNAi with 2X *Actin 5C*-Gal4 (UAS-*dPICK1* RNAi/*Actin 5C*-Gal4; *Actin 5C*-Gal4/UAS-*dICA69* RNAi). We found mild but not significant enhancement of NMJ morphological defects (2X *Actin 5C*-Gal4> *dRab2*, *dICA69* RNAi, 0.80±0.14; 2X *Actin 5C*-Gal4> *dPICK1*, *dICA69* RNAi, 0.80±0.11) (Fig. 6A-H). The NMJ morphological defects are not additive suggesting that ICA69, PICK1 and Rab2 possibly function in the same genetic pathway to regulate NMJ development in *Drosophila*.

In order to strengthen this conclusion, we analyzed the Spectrin cytoskeleton underlying the postsynaptic SSR by using an antibody against α-Spectrin. Consistent with our prediction, RNAi-mediated knockdown of PICK1 or Rab2 causes reduced levels of synaptic α-Spectrin similar to that observed in the *ICA69* mutant (Fig. 6I-L). These data strongly suggest that ICA69, PICK1 and Rab2 also regulate proper assembly of Spectrin cytoskeleton around the *Drosophila* SSR.

Rab2 regulates synaptic iGluR levels by regulating ICA69 at the NMJ

In order to gain further insights into the interrelationship between Rab2 and ICA69, we first analyzed the synaptic levels of iGluRs in

Development (2017) 144, 2032-2044 doi:10.1242/dev.145920

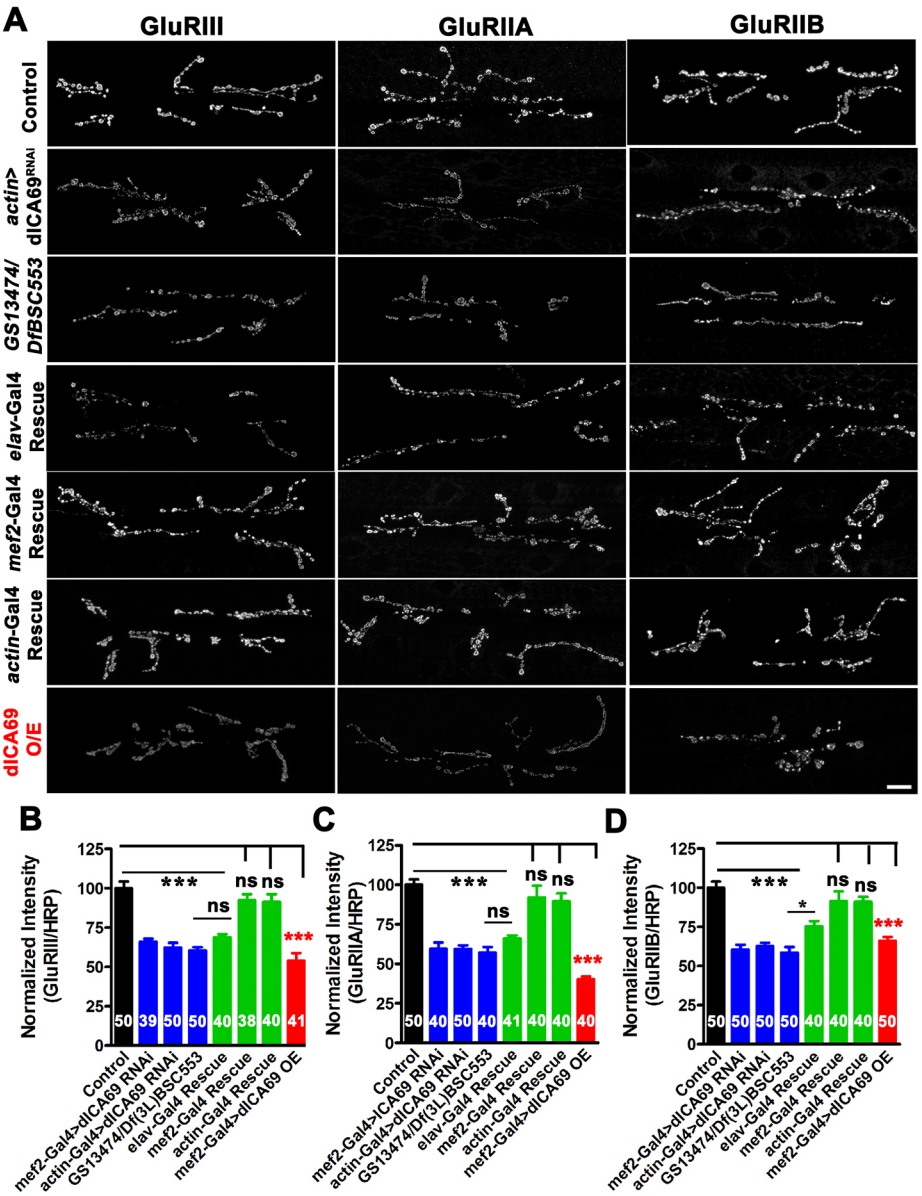

Fig. 4. ICA69 regulates GluRIIA and GluRIIB receptor clusters at the larval NMJ.
(A) Representative images of third instar larval NMJ synapses at muscle 6/7 labeled with GluRIII, GluRIIA or GluRIIB in control, *Actin 5C*-Gal4-driven *ICA69* RNAi, *GS13474/Df(3L)BSC553*, ICA69 transgene-rescued (*elav^{c155}/+; UAS-dICA69^{FL}/+; GS13474/Df(3L)BSC553* or *UAS-dICA69^{FL}/+; mef2-Gal4, Df(3L)BSC553/GS13474* or *UAS-dICA69^{FL}/+; Actin 5C-Gal4, Df(3L)BSC553/GS13474*) and *mef2*-Gal4-driven ICA69 overexpressing (O/E) (*UAS-dICA69^{FL}/+; mef2*-Gal4/+) animals. Note that the iGluR levels in the *ICA69* mutant are restored to wild-type levels by expressing *ICA69* transgene in muscle but not in the neurons. Scale bar: 10 µm. (B-D) Histograms showing quantification of synaptic GluR levels in the indicated genotypes. ***P<0.0001; ns, not significant. Error bars represent mean±s.e.m. Statistical analysis based on one-way ANOVA with post-hoc Tukey's test for multiple comparisons.

Actin 5C-Gal4-driven *Rab2* RNAi animals. Interestingly, we found that knockdown of *Rab2* dramatically reduces synaptic levels of GluRIII (Fig. 7A,B,E-G) suggesting that both GluRIIA and GluRIIB receptor clusters are reduced at the NMJ. Similarly, overexpressing GDP-locked Rab2DN (YFP-Rab2^{S20N}) also reduced the synaptic targeting/retention of glutamate receptors (Fig. 7C,E-G). Interestingly, overexpressing GTP-locked Rab2CA (YFP-Rab2^{Q65L}) showed mild but significant increases in GluRIII, GluRIIB and GluRIIA levels at *Drosophila* NMJ (Fig. 7D,E-G). Taken together, these data suggest that Rab2 regulates glutamate receptor clustering at the *Drosophila* NMJ.

As ICA69 is an effector of Rab2 (Buffa et al., 2008) and downregulation of Rab2 phenocopied NMJ morphological defects as well as affecting iGluR targeting/retention, we next determined whether the synaptic iGluR level regulated by Rab2 is mediated through ICA69. Interestingly, we found a dramatic reduction in synaptic ICA69 level at the NMJ in animals expressing *Rab2* RNAi (Fig. 7H-K). Similar results were obtained when GDP-locked Rab2DN was expressed (data not shown). However, levels of Rab2 remained unaltered in animals expressing *ICA69* RNAi (data not shown). Taken together, these data suggest that Rab2 regulates synaptic ICA69 levels, which in turn facilitate targeting/retention of various iGluR subunits at the *Drosophila* NMJ. Because we found that Rab2 affected ICA69 levels, we next assessed whether Rab2 was located at the NMJs. We analyzed the expression of Rab2^{EYFP} expressed under the control of Rab2 regulatory sequences. We found that Rab2 is localized both within the bouton as well as in the muscles, where it appears as punctate structures (Fig. 7L-N). This suggests that Rab2 could regulate trafficking of ICA69 to the SSRs.

In order to further strengthen our observation that Rab2 functions through ICA69, we co-expressed an *ICA69* transgene in a *Rab2*-RNAi background (*UAS-dICA69^{FL}/Actin 5C-Gal4; UAS-Rab2 RNAi/Actin 5C-Gal4*). Interestingly, the morphological defects, as well as synaptic iGluR levels, were fully restored when the ICA69 transgene was co-expressed with *Rab2* RNAi (Fig. 8A-M). Moreover, the synaptic levels of ICA69 were also restored to the wild-type levels (Fig. 8I). Taken together, these data suggest that Rab2 regulates structural organization of NMJ through ICA69 and functions genetically upstream of ICA69.

Development (2017) 144, 2032-2044 doi:10.1242/dev.145920

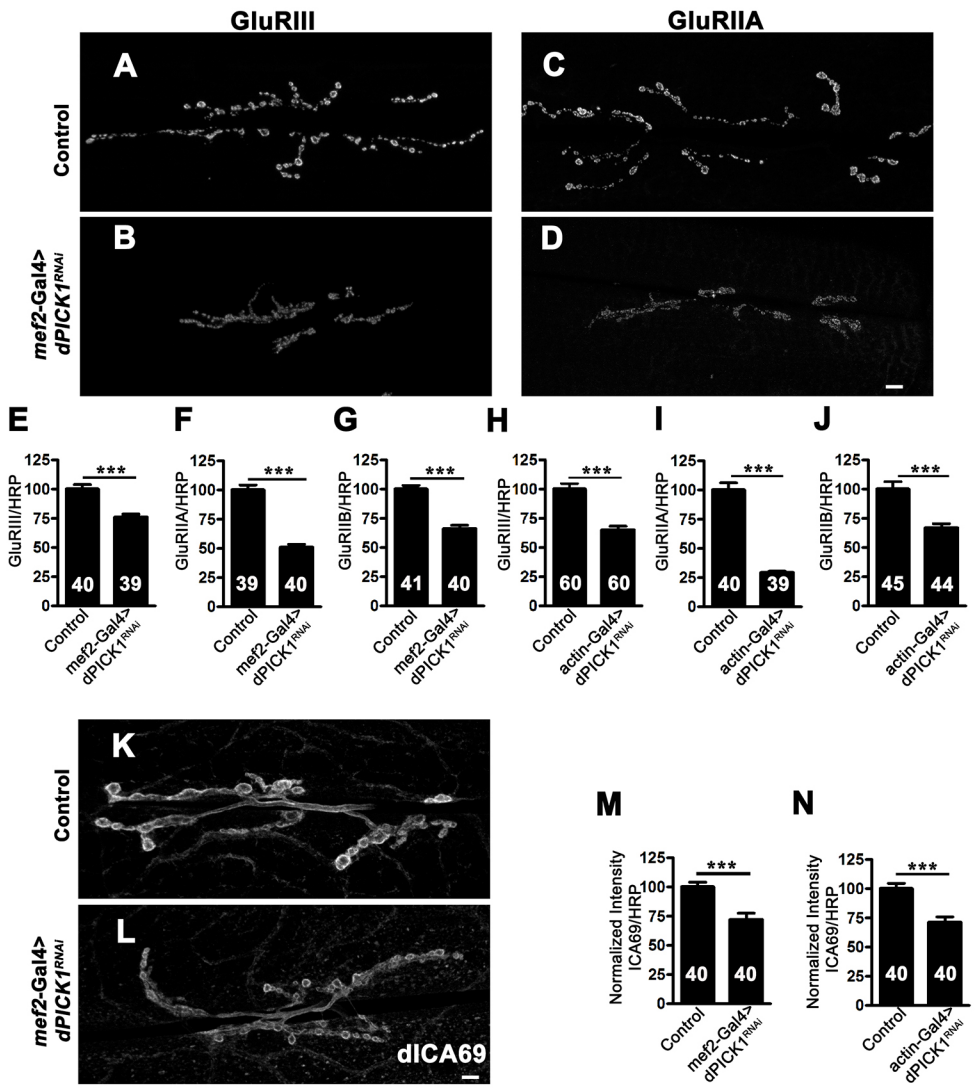

Fig. 5. RNAi-mediated knockdown of PICK1 reduces synaptic iGluR levels. (A-D) Confocal images of muscle 6/7 NMJ synapses in control and *mef2*-Gal4-driven *PICK1* RNAi animals labeled with GluRIII or GluRIIA antibodies. Scale bar: 15 µm. (E-G) Histogram showing normalized average synaptic fluorescence level of GluRIII (E), GluRIIA (F) and GluRIIB (G) in control and *mef2*-Gal4-driven *PICK1* RNAi animals. (H-J) Histogram showing normalized average synaptic fluorescence level of GluRIII (H) GluRIIA, (I) and GluRIIB (J) in control and *Actin 5C*-Gal4-driven *PICK1* RNAi animals. (K,L) Confocal images of muscle 6/7 NMJ synapses in control (K) and *mef2*-Gal4-driven *PICK1* RNAi (L) animals immunolabeled with ICA69 antibody. Scale bar: 10 µm. (M,N) Histograms showing normalized average synaptic fluorescence level of ICA69 in control and *mef2*-Gal4-driven *PICK1* RNAi (M) or *Actin 5C*-Gal4-driven *PICK1* RNAi (N) animals. ***P<0.0001. Error bars represent mean±s.e.m. calculated using Student's two-tailed t-test.

DISCUSSION

In this study, we demonstrate that ICA69 regulates NMJ structural organization and synaptic levels of glutamate receptor clusters. Our findings suggest a model in which Rab2 functions genetically upstream of ICA69 to regulate its synaptic level, which in turn regulates the Spectrin cytoskeleton and iGluRs at the NMJ (Fig. 8N).

Regulation of NMJ organization by *Drosophila* ICA69

The requirement of ICA69 for *Drosophila* NMJ organization is strongly supported by its enrichment in the postsynaptic Spectrin-rich scaffold. Consistent with this idea, *ICA69* mutants or animals with downregulated ICA69 levels show reduced arborization and bouton numbers at the NMJ. Several studies have shown that cytoskeletal regulation is a key process for NMJ development (Coyle et al., 2004; Koch et al., 2014; Rodal et al., 2008; Zhao et al., 2013). Multiple lines of evidence suggest that ICA69 promotes NMJ growth by regulating the cytoskeletal network surrounding the SSR. First, ICA69 is highly enriched at the NMJ in the same microdomain as Spectrin. Second, ICA69 induces filopodia in cultured cells and relocalizes positive regulators of actin polymerization at the filopodia. Third, mutation in ICA69 significantly reduces α-Spectrin levels. The Actin-Spectrin scaffold at the postsynapse has been implicated in regulation of NMJ organization in postembryonic development in *Drosophila* (Featherstone et al., 2001; Pielage et al., 2006). Our study reveals a crucial requirement of ICA69 in regulating synaptic α-Spectrin levels and indicates that ICA69 is required for the assembly of Actin-Spectrin scaffolds surrounding the SSR. Whether localization and/or stability of postsynaptic Spectrin-Actin scaffold depends on direct interaction between scaffold components and ICA69 or on some unknown signaling mechanism needs to be further investigated.

For the proper establishment of NMJ connections, neurons as well as muscles require trafficking of various synaptic proteins. Rab GTPases and their regulators are considered to be some of the most important signaling molecules for intracellular trafficking (Khodosh et al., 2006; Lee et al., 2013; Zou et al., 2015). Interestingly, nearly half of all the *Drosophila* Rab proteins function specifically in neurons and a few of them localize to the NMJs (Bae et al., 2016; Chan et al., 2011; Gillingham et al., 2014; West et al., 2015). ICA69 physically associates with Rab2 (Buffa et al., 2008) and has been suggested as one of its effectors in regulating dense core vesicle maturation in *Caenorhabditis elegans* (Sumakovic et al., 2009). We found that *Rab2* endogenous regulatory sequence-driven $Rab2^{EYFP}$ is detectable in the larval muscles as punctate structures, suggesting its involvement in NMJ organization. This idea is supported by four compelling pieces of evidence. First, ubiquitous or muscle-specific

Development (2017) 144, 2032-2044 doi:10.1242/dev.145920

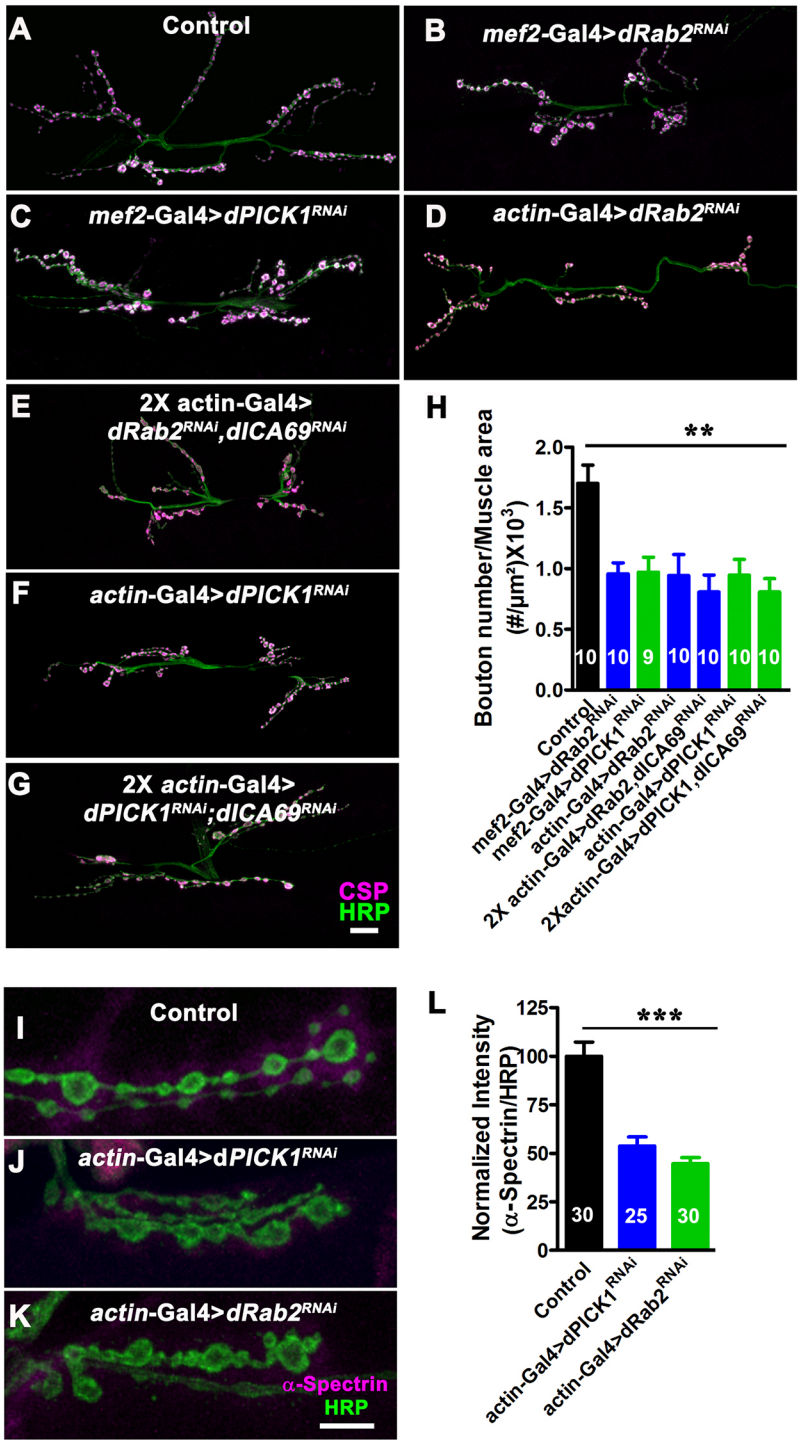

Fig. 6. Knockdown of PICK1 or Rab2 phenocopies *ICA69* mutation. (A-G) Confocal images of muscle 6/7 NMJ synapses in control (A), *mef2*-Gal4-driven *Rab2* RNAi (B), *mef2*-Gal4-driven *PICK1* RNAi (C), *Actin 5C*-Gal4-driven *Rab2* RNAi (D), 2X *Actin 5C*-Gal4-driven *Rab2* RNAi, *ICA69* RNAi (*Actin 5C-Gal4/+;UAS-dRab2RNAi/UAS-dICA69 RNAi,Actin 5C-Gal4*) (E), *Actin 5C*-Gal4-driven *PICK1* RNAi (F) and 2X *Actin 5C*-Gal4-driven *PICK1* RNAi; *ICA69* RNAi (*UAS-dPICK1 RNAi/ Actin 5C-Gal4; Actin 5C-Gal4/UAS-dICA69 RNAi*) (G) animals co-labeled with HRP (green) and CSP (magenta) antibodies. Scale bar: 20 µm. (H) Histogram showing average number of boutons at muscle 6/7 of the A2 hemisegment in control (1.70±0.15), *mef2*-Gal4-driven *Rab2* RNAi (0.95±0.09), *mef2*-Gal4-driven *PICK1* RNAi (0.97±0.12), *Actin 5C*-Gal4-driven *Rab2* RNAi (0.94±0.17), 2X *Actin 5C*-Gal4-driven *Rab2* RNAi, *ICA69* RNAi (0.80±0.14), *Actin 5C*-Gal4-driven *PICK1* RNAi (0.94±0.12) and 2X *Actin 5C*-Gal4-driven *PICK*1 RNAi; *ICA69* RNAi (0.80±0.11) animals. (I-K) Confocal images of third instar larval NMJ synapses in control (I), *Actin 5C*-Gal4-driven *PICK1* RNAi (J) and *Actin 5C*-Gal4-driven *Rab2* RNAi (K) synapses, immunostained with anti-HRP (green) and anti-α-Spectrin (magenta) antibodies. Scale bar: 5 µm. (L) Histogram showing synaptic levels of α-Spectrin in the indicated genotypes. Compared with controls (100±7.34), *Actin 5C*-Gal4-driven *PICK1* RNAi (53.71±4.67) and *Actin 5C*-Gal4-driven *Rab2* RNAi (44.63±3.15) synapses showed significant reduction in α-Spectrin level. ***P*<0.001, ****P*<0.0001. Error bar represents mean±s.e.m. Statistical analysis based on one-way ANOVA with post-hoc Tukey's test for multiple comparisons.

knockdown of *Rab2* phenocopies *ICA69* mutants. Second, knockdown of *Rab2* significantly reduces synaptic α-Spectrin levels. Third, Rab2 directly regulates synaptic ICA69 levels. Fourth, co-expressing an *ICA69* transgene and *Rab2* RNAi rescues the morphological defects of *Rab2* RNAi. Based on these observations, we suggest that *Drosophila* Rab2 functions genetically upstream of ICA69. Like Rab2, PICK1 depletion reduced synaptic ICA69 levels and phenocopied the NMJ morphological defects observed in *ICA69* mutants or after Rab2 depletion. Moreover, simultaneous knockdown of ICA69 and PICK1 or of ICA69 and Rab2 did not show an additive effect on the NMJ structural defects. These observations support the notion that ICA69, PICK1 and Rab2 might function in the same genetic pathway to regulate NMJ structural organization.

Regulation of glutamate receptor clusters by ICA69

In mammalian neurons, ICA69 is, surprisingly, not enriched at the synapses and negatively regulates AMPA receptor trafficking (Cao et al., 2007). Hence, we expected that *ICA69* mutants would have normal, if not more, iGluR clusters at the NMJ. Contrary to this expectation, we found that reducing the ICA69 level resulted in reduced GluRIIA as well as GluRIIB glutamate receptor clusters. A

Development (2017) 144, 2032-2044 doi:10.1242/dev.145920

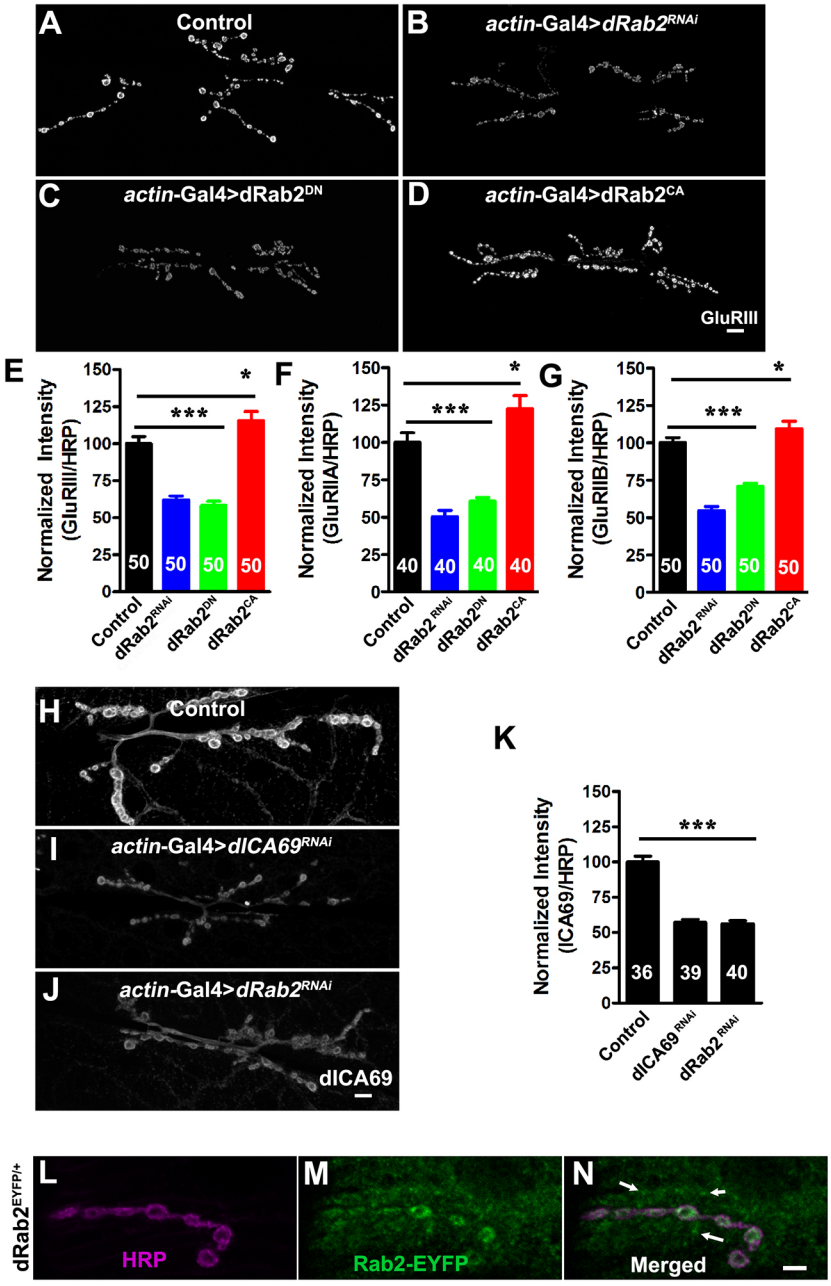

Fig. 7. Rab2 regulates iGluR clusters as well as ICA69 levels at the *Drosophila* NMJ. (A-D) Confocal images of muscle 6/7 NMJ synapses in control (A), *Actin 5C*-Gal4-driven *Rab2* RNAi (B), *Actin 5C*-Gal4-driven dominant negative Rab2 (C) and *Actin 5C*-Gal4-driven constitutive active form of Rab2 (D) labeled with GluRIII antibodies. Scale bar: 15 µm. (E-G) Histograms showing normalized average synaptic fluorescence level of GluRIII (E), GluRIIA (F) and GluRIIB (G) in control, *Actin 5C*-Gal4-driven *Rab2* RNAi, *Actin 5C*-Gal4-driven dominant negative Rab2 and *Actin 5C*-Gal4-driven constitutive active form of Rab2. (H-J) Confocal images of muscle 6/7 NMJ synapses in control (H), *Actin 5C*-Gal4-driven *ICA69* RNAi (I) and *Actin 5C*-Gal4-driven *Rab2* RNAi (J) animals labeled with ICA69 antibody. Scale bar: 15 µm. (K) Histogram showing normalized average synaptic fluorescence level of ICA69 in control, *Actin 5C*-Gal4-driven ICA69 RNAi and *Actin 5C*-Gal4-driven *Rab2* RNAi animals. (L-N) Confocal image of boutons at third instar larval NMJ synapse expressing EYFP-tagged Rab2 (Rab2 ^{EYFP}/+) double immunolabeled with anti-HRP (magenta) and anti-GFP (green). Note that Rab2 is localized both pre- and postsynaptically at the NMJ. Arrows in N indicate the punctate distribution of Rab2 in the muscle. Scale bar: 5 µm. *P<0.05; ***P<0.0001. Error bars represent mean±s.e.m. Statistical analysis based on one-way ANOVA with post-hoc Tukey's test for multiple comparisons.

recent study has shown that ICA69 and PICK1 stability is interdependent in *Drosophila* brain (Cao et al., 2013). Thus, it is likely that iGluR clusters at the NMJ are regulated by levels of ICA69 and PICK1 in muscles.

How does ICA69 reduce iGluR levels both in knockdown and overexpression scenarios? We suggest that the endogenous stoichiometry of ICA69 and PICK1 is crucial for normal synaptic targeting of iGluRs at the *Drosophila* NMJ. Reducing ICA69 destabilizes the ICA69-PICK1 heteromeric complex thereby reducing PICK1 availability for synaptic targeting of iGluRs. Overexpression of ICA69 forms more of the ICA69-PICK1 inhibitory complexes, which reduces synaptic targeting of iGluRs. Hence, we support the idea that the endogenous level of ICA69 is crucial for maintaining normal glutamate receptor clusters at the synapses.

Our data suggest that ∼40% simultaneous reduction of GluRIIA/IIB/III at *Drosophila* NMJ synapses has no major consequence on larval synaptic physiology. We suggest three possibilities to explain this. First, the relative levels of GluRIIA and GluRIIB subunits are crucial for determining the efficacy of synaptic transmission at the *Drosophila* NMJ synapse (Marrus et al., 2004). The decrease for each of the GluRIIA, -IIB and -III subunits in the *ICA69* mutant is almost identical; ∼40% compared with controls. This hints towards a homeostatic compensatory mechanism whereby ∼60% of the receptor subunits are sufficient to form enough functional receptor complexes, which can maintain normal synaptic strength. Second, the amount of GluRIII is reflective of the sum of GluRIIA and -IIB complexes together, and GluRIII is essential for the localization of GluRIIA and IIB subunits (Qin et al., 2005). A 40% decrease in GluRIII staining correlates well with an identical decrease in GluRIIA and -IIB staining. It is plausible that there is essentially negligible change in functional glutamate receptor assembly at *ICA69* mutant synapses. Third,

Development (2017) 144, 2032-2044 doi:10.1242/dev.145920

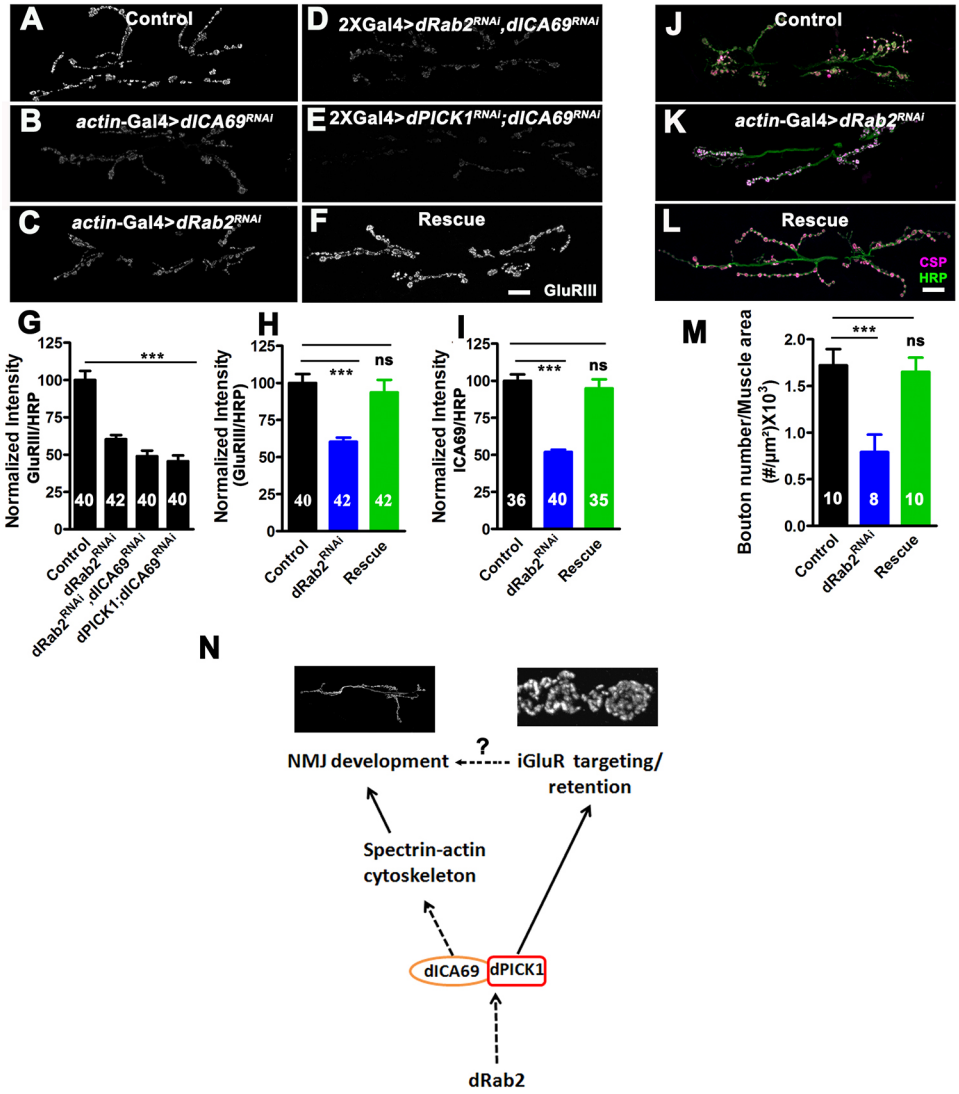

Fig. 8. Rab2 functions through ICA69 to regulate NMJ organization. (A-F) Confocal images of muscle 6/7 NMJ synapses in control (A), *Actin 5C*-Gal4-driven *ICA69* RNAi (B) and *Actin 5C*-Gal4-driven *Rab2* RNAi (C), 2X *Actin 5C*-Gal4-driven *Rab2* RNAi, *ICA69* RNAi (*Actin 5C-Gal4/+;UAS-dRab2 RNAi/UAS-dICA69 RNAi,Actin 5C-Gal4*) (D), 2X *Actin 5C*-Gal4-driven *PICK1* RNAi, *ICA69* RNAi (*UAS-dPICK1 RNAi/Actin 5C-Gal4;Actin 5C-Gal4/UAS-dICA69 RNAi*) (E) and rescue (*UAS-dICA69^{FL}/Actin 5C-Gal4;UAS-dRab2 RNAi/Actin 5C-Gal4*) (F) animals labeled with GluRIII antibody. Scale bar: 15 µm. (G) Histogram showing normalized average synaptic fluorescence of GluRIII in control, *Actin 5C*-Gal4-driven *Rab2* RNAi, 2X *Actin 5C*-Gal4-driven *Rab2* RNAi, *ICA69* RNAi (*Actin 5C-Gal4/+;UAS-dRab2 RNAi/UAS-dICA69 RNAi,Actin 5C-Gal4*) and 2X *Actin 5C*-Gal4-driven *PICK1* RNAi, *ICA69* RNAi (*UAS-dPICK1 RNAi/Actin 5C-Gal4; Actin 5C-Gal4/UAS-dICA69 RNAi*) animals. (H) Histogram showing normalized average synaptic fluorescence of GluRIII in control, *Actin 5C*-Gal4-driven *Rab2* RNAi and animals co-expressing *ICA69* transgene and *Rab2* RNAi (*UAS-dICA69^{FL}/Actin 5C-Gal4;UAS-dRab2 RNAi/Actin 5C-Gal4*). (I) Histogram showing normalized average synaptic fluorescence of ICA69 in control, *Actin 5C*-Gal4-driven *Rab2* RNAi and animals co-expressing ICA69 transgene and *Rab2* RNAi (*UAS-dICA69^{FL}/Actin 5C-Gal4;UAS-dRab2 RNAi/Actin 5C-Gal4*). (J-L) Confocal images of muscle 6/7 NMJ synapses in control (J), *Actin 5C*-Gal4-driven *Rab2* RNAi (K) and animals co-expressing ICA69 transgene and *Rab2* RNAi (*UAS-dICA69^{FL}/Actin 5C-Gal4;UAS-dRab2 RNAi/Actin 5C-Gal4*) (L) co-labeled with HRP (green) and CSP (magenta) antibodies. Scale bar: 15 µm. (M) Histogram showing normalized bouton number at muscle 6/7 of the A2 hemisegment in control (1.72±0.17), *Actin 5C*-Gal4-driven *Rab2* RNAi (0.79±0.18) and animals co-expressing ICA69 transgene and *Rab2* RNAi (rescue) (*UAS-dICA69^{FL}/Actin 5C-Gal4; UAS-dRab2 RNAi/Actin 5C-Gal4*) (1.65±0.15). (N) A model depicting regulation of NMJ structural organization by Rab2 through the ICA69-PICK1 complex. Rab2 functions genetically upstream of ICA69 and regulates its stability. ICA69 and PICK1, but not Rab2, are interdependent for their stability. At the NMJ, this complex regulates two aspects of its organization: (1) it regulates NMJ structural development possibly by modulating the Actin-Spectrin cytoskeleton surrounding the SSR and (2) it regulates synaptic targeting/retention of both GluRIIA and GluRIIB receptor clusters at the NMJ. The synaptic level of glutamate receptors might also affect NMJ development possibly by regulating retrograde synaptic signaling or by inducing motor activity. ***P<0.0001; ns, not significant. Error bars represent mean±s.e.m. Statistical analysis based on one-way ANOVA with post-hoc Tukey's test for multiple comparisons.

ICA69 possibly plays a role in trafficking glutamate receptors to the postsynaptic density and is not rate limiting in the formation of functional glutamate receptor complexes. Thus, *ICA69* mutants exhibit normal synaptic physiology without embracing other compensatory mechanisms such as reduced quantal size or increased quantal content.

How might the iGluR levels relate to the NMJ growth? A tight correlation exists between the amount of synaptic glutamate receptors and the NMJ morphology. Downregulation of iGluRs in muscles has been shown to reduce the number of boutons (Sulkowski et al., 2014). Similarly, hypomorphic mutants of GluRIII or GluRIIA have reduced bouton numbers (Sulkowski

Development (2017) 144, 2032-2044 doi:10.1242/dev.145920

et al., 2014). Consistent with this, overexpression of GluRIIA induces arborization and bouton number (Sigrist et al., 2002). Moreover, mutants with altered synaptic iGluR levels also show altered bouton numbers. For instance, *neto* and *filamin* (*cheerio*) mutants show reduced iGluR levels and bouton numbers (Kim et al., 2012; Lee and Schwarz, 2016). One of the possible mechanisms by which glutamate receptors can alter the NMJ morphology is through regulation of synaptic phospho-MAD levels (Sulkowski et al., 2014). As the iGluRs (for instance, GluRIID) have also been shown to localize in central neuropil (Featherstone et al., 2005), it remains a possibility that the endogenous pattern of central electrical activity could also play crucial roles in sculpting the NMJ during development.

MATERIALS AND METHODS

Bioinformatics analysis

A protein-to-protein BLAST was performed for known human BAR-domain proteins with *Drosophila* proteins using BLAST-P algorithm of NCBI (www.ncbi.nlm.nih.gov). We shortlisted 25 BAR-domain proteins based on E-value, identity and similarity (Table S1). We obtained available RNAi lines against 19 of these genes from the Vienna *Drosophila* RNAi Center and the Bloomington *Drosophila* Stock Center for further analysis by knockdown experiments.

Drosophila stocks and genetics

Flies were reared at 25°C unless otherwise stated. All stocks and crosses were grown in standard cornmeal medium. Flies for RNAi-mediated knockdown experiments were grown at 28°C. The following *Drosophila* lines were used in this study: *Df(3L)BSC553*, *Df(3L)BSC449*, Rab2-EYFP (Dunst et al., 2015) (BL-62540), *UASp-YFP-dRab2*^{Q65L} (BL-9760), *UASt-YFP-dRab2*^{S20N} (BL-23640), *Rab2* RNAi (BL-34922), *ICA69* RNAi line (27181/GD), *PICK1* RNAi (104486/KK) and P-element insertion mutants, *GS14708* and *GS13474* (*Drosophila* Genomics Resource Center, Kyoto Stock Center, Japan). The Gal4 driver lines used in this study were muscle-specific *mef2*-Gal4, pan neural *elav*^{C155}-Gal4 and ubiquitous *Actin 5C*-Gal4. All controls used in this study were *w*^{1118} unless stated otherwise.

Generation of ICA69 transgenic flies

The open reading frame of ICA69 was amplified from cDNA using gene-specific primers (Table S2), cloned into the pUAST vector and injected into *Drosophila* embryos for transgenesis.

Semiquantitative and quantitative real-time PCR

One microgram of total RNA isolated from larval fillets was used to synthesize cDNA using Superscript II reverse transcriptase (Life Technologies). PCR reactions were set up using gene-specific primers and reactions were stopped every two cycles after 25 cycles. *Rp49* (*RpL32*) was used as internal RNA loading control. For qPCR, one-tenth volume of the cDNA was used for real-time PCR with the CFX-Connect Real-Time System (Bio-Rad). Sybr Green was used for detecting mRNA with a final primer concentration of 200 nM. qRT- PCR for each sample was performed in triplicate and the fold-change was calculated using the $2^{-\Delta(\Delta Ct)}$ method. The sequences of primers used for qRT-PCR are listed in Table S2.

Antibodies and immunochemistry

Larvae were dissected in calcium-free HL3 saline and fixed in 4% paraformaldehyde. Anti-ICA69 antibody was used at 1:600 for immunostaining. The monoclonal antibodies anti-Dlg, anti-GluRIIA, anti-CSP, anti-Synapsin, anti-actin and anti-α-Spectrin were obtained from the Developmental Studies Hybridoma Bank and were used at 1:50. Other antibodies used were anti-GluRIIB (Marrus and DiAntonio, 2004), GluRIII (Marrus et al., 2004), Wasp (Bogdan et al., 2005) and SCAR (Zallen et al., 2002). Fluorophore-coupled secondary antibodies were used at 1:800. DAPI and Alexa 488-conjugated anti-HRP were used at 1:2000 and 1:800, respectively. See the supplementary Materials and Methods for more details.

Western blotting

Third instar larval body wall muscle preparations were homogenized in 1× SDS sample buffer (50 mM Tris-HCl, pH 6.8; 2% SDS, 2% β-mercaptoethanol, 0.1% Bromophenol Blue and 10% glycerol), boiled and centrifuged at 3000 ***g***. Approximately 600 µg protein was separated on 12% SDS-PAGE and then transferred to Hybond-PVDF-LFP membrane (Amersham, GE Healthcare Life Sciences). The membrane was blocked with 5% skimmed milk for 1 h at room temperature and then incubated with anti-ICA69 (1:5000) at 4°C overnight followed by 1 h incubation with HRP-conjugated secondary antibody at 1:10,000. Signals were detected using the ECL-plus detection system (Amersham, GE Healthcare Life Sciences) according to the manufacturer's recommendations.

Synthetic liposomes and membrane tubulation

Synthetic liposomes were prepared by mixing DOPC, DOPS, PI(4,5)P2 and Rhodamine-PE (Avanti Polar Lipids) as previously described (Peter et al., 2004). Vesicles were extruded through a polycarbonate filter with a pore size of 100 nm to yield uniform diameter liposomes. GST or GST-ICA69$^{N\text{-}BAR}$ were incubated with liposomes on a glass slide and imaged (Cascade 512SC EMCCD camera mounted on an Axio Examiner D1 microscope) at 10 min and 30 min.

Electrophysiology

For electrophysiology recordings, third instar larvae were dissected in Ca^{2+}-free HL3 and recordings were performed using sharp intracellular glass electrodes (15-20 MΩ) from A2 hemisegment, muscle 6 in 0.75 or 1.5 mM Ca^{2+}-containing HL3 as previously described (Choudhury et al., 2016).

Drosophila S2R+ cell culture and filopodia quantification

Drosophila S2R+ cells were cultured in 1× Schneider's Drosophila media (Invitrogen) supplemented with 10% fetal bovine serum, 50 U/ml penicillin, and 50 µg/ml streptomycin in 75-cm² T-flasks (BD Biosciences) at 25°C. The cells (~3×10³) were transiently co-transfected with pUAST-dICA69^{FL}, pUAST-dICA69^{BAR}, pUAST-dICA69^{ICAC} and *actin*-Gal4 (1 µg each) using Mirus *TransIT* transfection agent as described previously (Handu et al., 2015). For microscopy, S2R+ cells were spotted onto Concanavalin A (Sigma-Aldrich)-coated coverslips and imaged with a 63× objective. The total number of filopodia was counted manually by visualizing actin-positive protrusions emerging out from each cell. The circumference of each cell was measured by drawing a circle that touched all the protrusions. The total number of filopodia was normalized to the circumference of the cell and expressed as total number of filopodia per 100 µm.

Quantification and morphometric analysis

Fluorescence imaging was carried out using a laser scanning confocal microscope (LSM 780; Carl Zeiss). All the control and experimental samples were acquired at the same laser power and gain and were processed in the same way. Quantification of NMJ morphological features was performed at muscle 6/7 of abdominal segment 2. Bouton numbers were quantified using anti-HRP and anti-CSP staining from at least eight NMJ synapses. For quantification of fluorescence intensity, images were captured at 63×/1.4NA. Only type Ib terminal boutons from at least six NMJ synapses were used for quantification using ImageJ software (National Institutes of Health). The numbers on the columns represent the number of boutons used for quantification. One-way ANOVA with post-hoc Tukey's test for multiple comparisons was used for statistical analysis. The data are presented as mean±s.e.m.

Acknowledgements

We thank Aaron Diantonio and Peter Dijke for sharing antibodies; the Bloomington *Drosophila* Stock Center, Vienna *Drosophila* RNAi Center and *Drosophila* Genomics Resource Center for fly stocks and Developmental Studies Hybridoma Bank, University of Iowa for monoclonal antibodies. We thank Shanker Jha, Saumitra Dey Choudhury and Subhabrata Sanyal for many useful comments on the manuscript.

Competing interests

The authors declare no competing or financial interests.

Author contributions

Conceptualization: B.M., Z.M., V.K.; Methodology: B.M., M.K., P.K.V.; Formal analysis: B.M., V.K.; Investigation: B.M., M.K.D., Z.M., M.K.; Resources: P.K.V.; Writing - original draft: B.M., V.K.; Writing - review & editing: B.M., M.K.D., Z.M., V.K.; Supervision: V.K.; Project administration: V.K.; Funding acquisition: V.K.

Funding

This work was supported by project grants from the Department of Biotechnology Ministry of Science and Technology, Government of India (BT/PR-15163/GBD/27/349/2011) and the Science and Engineering Research Board (SR/FT/LS-103/2010 to V.K.), and intramural funds from the Indian Institute of Science Education and Research Bhopal.

Supplementary information

Supplementary information available online at
http://dev.biologists.org/lookup/doi/10.1242/dev.145920.supplemental

References

Aspenström, P. (2014). BAR domain proteins regulate Rho GTPase signaling. *Small GTPases* **5**, 7.

Bae, H., Chen, S., Roche, J. P., Ai, M., Wu, C., Diantonio, A. Graf, E. R. (2016). Rab3-GEF controls active zone development at the Drosophila neuromuscular junction. *eNeuro* **3**, ENEURO.0031-16.2016.

Bogdan, S., Stephan, R., Löbke, C., Mertens, A. and Klämbt, C. (2005). Abi activates WASP to promote sensory organ development. *Nat. Cell Biol.* **7**, 977-984.

Buffa, L., Fuchs, E., Pietropaolo, M., Barr, F. and Solimena, M. (2008). ICA69 is a novel Rab2 effector regulating ER-Golgi trafficking in insulinoma cells. *Eur. J. Cell Biol.* **87**, 197-209.

Cao, M., Xu, J., Shen, C., Kam, C., Huganir, R. L. and Xia, J. (2007). PICK1-ICA69 heteromeric BAR domain complex regulates synaptic targeting and surface expression of AMPA receptors. *J. Neurosci.* **27**, 12945-12956.

Cao, M., Mao, Z., Kam, C., Xiao, N., Cao, X., Shen, C., Cheng, K. K., Xu, A., Lee, K. M., Jiang, L. et al. (2013). PICK1 and ICA69 control insulin granule trafficking and their deficiencies lead to impaired glucose tolerance. *PLoS Biol.* **11**, e1001541.

Chan, C.-C., Scoggin, S., Wang, D., Cherry, S., Dembo, T., Greenberg, B., Jin, E. J., Kuey, C., Lopez, A., Mehta, S. Q. et al. (2011). Systematic discovery of Rab GTPases with synaptic functions in Drosophila. *Curr. Biol.* **21**, 1704-1715.

Chang, L., Kreko, T., Davison, H., Cusmano, T., Wu, Y., Rothenfluh, A. and Eaton, B. A. (2013). Normal dynactin complex function during synapse growth in Drosophila requires membrane binding by Arfaptin. *Mol. Biol. Cell* **24**, 1749-1764.

Choudhury, S. D., Mushtaq, Z., Reddy-Alla, S., Balakrishnan, S. S., Thakur, R. S., Krishnan, K. S., Raghu, P., Ramaswami, M. and Kumar, V. (2016). sigma2-adaptin facilitates basal synaptic transmission and is required for regenerating endo-exo cycling pool under high-frequency nerve stimulation in Drosophila. *Genetics* **203**, 369-385.

Coyle, I. P., Koh, Y.-H., Lee, W.-C., Slind, J., Fergestad, T., Littleton, J. T. and Ganetzky, B. (2004). Nervous wreck, an SH3 adaptor protein that interacts with Wsp, regulates synaptic growth in Drosophila. *Neuron* **41**, 521-534.

Dharmalingam, E., Haeckel, A., Pinyol, R., Schwintzer, L., Koch, D., Kessels, M. M. and Qualmann, B. (2009). F-BAR proteins of the syndapin family shape the plasma membrane and are crucial for neuromorphogenesis. *J. Neurosci.* **29**, 13315-13327.

DiAntonio, A. (2006). Glutamate receptors at the Drosophila neuromuscular junction. *Int. Rev. Neurobiol.* **75**, 165-179.

Dunst, S., Kazimiers, T., von Zadow, F., Jambor, H., Sagner, A., Brankatschk, B., Mahmoud, A., Spannl, S., Tomancak, P., Eaton, S. et al. (2015). Endogenously tagged rab proteins: a resource to study membrane trafficking in Drosophila. *Dev. Cell* **33**, 351-365.

Featherstone, D. E., Davis, W. S., Dubreuil, R. R. and Broadie, K. (2001). Drosophila alpha- and beta-spectrin mutations disrupt presynaptic neurotransmitter release. *J. Neurosci.* **21**, 4215-4224.

Featherstone, D. E., Rushton, E., Rohrbough, J., Liebl, F., Karr, J., Sheng, Q., Rodesch, C. K. and Broadie, K. (2005). An essential Drosophila glutamate receptor subunit that functions in both central neuropil and neuromuscular junction. *J. Neurosci.* **25**, 3199-3208.

Fricke, R., Gohl, C., Dharmalingam, E., Grevelhörster, A., Zahedi, B., Harden, N., Kessels, M., Qualmann, B. and Bogdan, S. (2009). Drosophila Cip4/Toca-1 integrates membrane trafficking and actin dynamics through WASP and SCAR/WAVE. *Curr. Biol.* **19**, 1429-1437.

Frost, A., Perera, R., Roux, A., Spasov, K., Destaing, O., Egelman, E. H., De Camilli, P. and Unger, V. M. (2008). Structural basis of membrane invagination by F-BAR domains. *Cell* **132**, 807-817.

Frost, A., Unger, V. M. and De Camilli, P. (2009). The BAR domain superfamily: membrane-molding macromolecules. *Cell* **137**, 191-196.

Gallo, G. (2013). Mechanisms underlying the initiation and dynamics of neuronal filopodia: from neurite formation to synaptogenesis. *Int. Rev. Cell Mol. Biol.* **301**, 95-156.

Gillingham, A. K., Sinka, R., Torres, I. L., Lilley, K. S. and Munro, S. (2014). Toward a comprehensive map of the effectors of rab GTPases. *Dev. Cell* **31**, 358-373.

Govek, E.-E., Newey, S. E., Akerman, C. J., Cross, J. R., Van der Veken, L. and Van Aelst, L. (2004). The X-linked mental retardation protein oligophrenin-1 is required for dendritic spine morphogenesis. *Nat. Neurosci.* **7**, 364-372.

Guerrier, S., Coutinho-Budd, J., Sassa, T., Gresset, A., Jordan, N. V., Chen, K., Jin, W. L., Frost, A. and Polleux, F. (2009). The F-BAR domain of srGAP2 induces membrane protrusions required for neuronal migration and morphogenesis. *Cell* **138**, 990-1004.

Habermann, B. (2004). The BAR-domain family of proteins: a case of bending and binding? *EMBO Rep.* **5**, 250-255.

Handu, M., Kaduskar, B., Ravindranathan, R., Soory, A., Giri, R., Elango, V. B., Gowda, H. and Ratnaparkhi, G. S. (2015). SUMO-Enriched proteome for Drosophila innate immune response. *G3 (Bethesda)* **5**, 2137-2154.

Harris, K. P. and Littleton, J. T. (2015). Transmission, development, and plasticity of synapses. *Genetics* **201**, 345-375.

He, J., Xia, M., Tsang, W. H., Chow, K. L. and Xia, J. (2015). ICA1L forms BAR-domain complexes with PICK1 and is crucial for acrosome formation in spermiogenesis. *J. Cell Sci.* **128**, 3822-3836.

Houy, S., Estay-Ahumada, C., Croise, P., Calco, V., Haeberle, A.-M., Bailly, Y., Billuart, P., Vitale, N., Bader, M.-F., Ory, S. et al. (2015). Oligophrenin-1 connects exocytotic fusion to compensatory endocytosis in neuroendocrine cells. *J. Neurosci.* **35**, 11045-11055.

Itoh, T., Erdmann, K. S., Roux, A., Habermann, B., Werner, H. and De Camilli, P. (2005). Dynamin and the actin cytoskeleton cooperatively regulate plasma membrane invagination by BAR and F-BAR proteins. *Dev. Cell* **9**, 791-804.

Jansen, A. M., Nässel, D. R., Madsen, K. L., Jung, A. G., Gether, U. and Kjaerulff, O. (2009). PICK1 expression in the Drosophila central nervous system primarily occurs in the neuroendocrine system. *J. Comp. Neurol.* **517**, 313-332.

Kessels, M. M. and Qualmann, B. (2006). Syndapin oligomers interconnect the machineries for endocytic vesicle formation and actin polymerization. *J. Biol. Chem.* **281**, 13285-13299.

Kessels, M. M. and Qualmann, B. (2015). Different functional modes of BAR domain proteins in formation and plasticity of mammalian postsynapses. *J. Cell Sci.* **128**, 3177-3185.

Khodosh, R., Augsburger, A., Schwarz, T. L. and Garrity, P. A. (2006). Bchs, a BEACH domain protein, antagonizes Rab11 in synapse morphogenesis and other developmental events. *Development* **133**, 4655-4665.

Kim, Y. J., Bao, H., Bonanno, L., Zhang, B. and Serpe, M. (2012). Drosophila Neto is essential for clustering glutamate receptors at the neuromuscular junction. *Genes Dev.* **26**, 974-987.

Koch, N., Kobler, O., Thomas, U., Qualmann, B. and Kessels, M. M. (2014). Terminal axonal arborization and synaptic bouton formation critically rely on abp1 and the arp2/3 complex. *PLoS One* **9**, e97692.

Lee, G. and Schwarz, T. L. (2016). Filamin, a synaptic organizer in Drosophila, determines glutamate receptor composition and membrane growth. *Elife* **5**, e19991.

Lee, M.-J., Jang, S., Nahm, M., Yoon, J.-H. and Lee, S. (2013). Tbc1d15-17 regulates synaptic development at the Drosophila neuromuscular junction. *Mol. Cells* **36**, 163-168.

Liu, S., Xiong, X., Zhao, X., Yang, X. and Wang, H. (2015). F-BAR family proteins, emerging regulators for cell membrane dynamic changes-from structure to human diseases. *J. Hematol. Oncol.* **8**, 47.

Marrus, S. B. and DiAntonio, A. (2004). Preferential localization of glutamate receptors opposite sites of high presynaptic release. *Curr. Biol.* **14**, 924-931.

Marrus, S. B., Portman, S. L., Allen, M. J., Moffat, K. G. and DiAntonio, A. (2004). Differential localization of glutamate receptor subunits at the Drosophila neuromuscular junction. *J. Neurosci.* **24**, 1406-1415.

Masuda, M., Takeda, S., Sone, M., Ohki, T., Mori, H., Kamioka, Y. and Mochizuki, N. (2006). Endophilin BAR domain drives membrane curvature by two newly identified structure-based mechanisms. *EMBO J.* **25**, 2889-2897.

Murakoshi, H., Wang, H. and Yasuda, R. (2011). Local, persistent activation of Rho GTPases during plasticity of single dendritic spines. *Nature* **472**, 100-104.

Nadif Kasri, N., Nakano-Kobayashi, A., Malinow, R., Li, B. and Van Aelst, L. (2009). The Rho-linked mental retardation protein oligophrenin-1 controls synapse maturation and plasticity by stabilizing AMPA receptors. *Genes Dev.* **23**, 1289-1302.

Nahm, M., Long, A. A., Paik, S. K., Kim, S., Bae, Y. C., Broadie, K. and Lee, S. (2010). The Cdc42-selective GAP rich regulates postsynaptic development and retrograde BMP transsynaptic signaling. *J. Cell Biol.* **191**, 661-675.

Nelson, J. C., Stavoe, A. K. H. and Colón-Ramos, D. A. (2013). The actin cytoskeleton in presynaptic assembly. *Cell Adh. Migr.* **7**, 379-387.

Peter, B. J., Kent, H. M., Mills, , I. G., , Vallis, Y., Butler, P. J., Evans, P. R. and McMahon, H. T. (2004). BAR domains as sensors of membrane curvature: the amphiphysin BAR structure. *Science* **303**, 495-499.

Pielage, J., Fetter, R. D. and Davis, G. W. (2006). A postsynaptic spectrin scaffold defines active zone size, spacing, and efficacy at the Drosophila neuromuscular junction. *J. Cell Biol.* **175**, 491-503.

Development (2017) 144, 2032-2044 doi:10.1242/dev.145920

Pietropaolo, M., Castaño, L., Babu, S., Buelow, R., Kuo, Y. L., Martin, S., Martin, A., Powers, A. C., Prochazka, M., Naggert, J. et al. (1993). Islet cell autoantigen 69 kD (ICA69). Molecular cloning and characterization of a novel diabetes-associated autoantigen. *J. Clin. Invest.* **92**, 359-371.

Pilon, M., Peng, X.-R., Spence, A. M., Plasterk, R. H. A. and Dosch, H.-M. (2000). The diabetes autoantigen ICA69 and its Caenorhabditis elegans homologue, ric-19, are conserved regulators of neuroendocrine secretion. *Mol. Biol. Cell* **11**, 3277-3288.

Qin, G., Schwarz, T., Kittel, R. J., Schmid, A., Rasse, T. M., Kappei, D., Ponimaskin, E., Heckmann, M. and Sigrist, S. J. (2005). Four different subunits are essential for expressing the synaptic glutamate receptor at neuromuscular junctions of Drosophila. *J. Neurosci.* **25**, 3209-3218.

Qualmann, B. and Kelly, R. B. (2000). Syndapin isoforms participate in receptor-mediated endocytosis and actin organization. *J. Cell Biol.* **148**, 1047-1062.

Rao, Y., Ma, Q., Vahedi-Faridi, A., Sundborger, A., Pechstein, A., Puchkov, D., Luo, L., Shupliakov, O., Saenger, W. and Haucke, V. (2010). Molecular basis for SH3 domain regulation of F-BAR-mediated membrane deformation. *Proc. Natl. Acad. Sci. USA* **107**, 8213-8218.

Rikhy, R., Kumar, V., Mittal, R. and Krishnan, K. S. (2002). Endophilin is critically required for synapse formation and function in Drosophila melanogaster. *J. Neurosci.* **22**, 7478-7484.

Rodal, A. A., Motola-Barnes, R. N. and Littleton, J. T. (2008). Nervous wreck and Cdc42 cooperate to regulate endocytic actin assembly during synaptic growth. *J. Neurosci.* **28**, 8316-8325.

Shen, K. and Scheiffele, P. (2010). Genetics and cell biology of building specific synaptic connectivity. *Annu. Rev. Neurosci.* **33**, 473-507.

Sigrist, S. J., Thiel, P. R., Reiff, D. F. and Schuster, C. M. (2002). The postsynaptic glutamate receptor subunit DGluR-IIA mediates long-term plasticity in Drosophila. *J. Neurosci.* **22**, 7362-7372.

Stanishneva-Konovalova, T. B., Kelley, C. F., Eskin, T. L., Messelaar, E. M., Wasserman, S. A., Sokolova, O. S. and Rodal, A. A. (2016). Coordinated autoinhibition of F-BAR domain membrane binding and WASp activation by Nervous Wreck. *Proc. Natl. Acad. Sci. USA* **113**, E5552-E5561.

Sulkowski, M., Kim, Y.-J. and Serpe, M. (2014). Postsynaptic glutamate receptors regulate local BMP signaling at the Drosophila neuromuscular junction. *Development* **141**, 436-447.

Sumakovic, M., Hegermann, J., Luo, L., Husson, S. J., Schwarze, K., Olendrowitz, C., Schoofs, L., Richmond, J. and Eimer, S. (2009). UNC-108/RAB-2 and its effector RIC-19 are involved in dense core vesicle maturation in Caenorhabditis elegans. *J. Cell Biol.* **186**, 897-914.

Ukken, F. P., Bruckner, J. J., Weir, K. L., Hope, S. J., Sison, S. L., Birschbach, R. M., Hicks, L., Taylor, K. L., Dent, E. W., Gonsalvez, G. B. et al. (2016). BAR-SH3 sorting nexins are conserved interacting proteins of Nervous wreck that organize synapses and promote neurotransmission. *J. Cell Sci.* **129**, 166-177.

West, R. J. H., Lu, Y., Marie, B., Gao, F.-B. and Sweeney, S. T. (2015). Rab8, POSH, and TAK1 regulate synaptic growth in a Drosophila model of frontotemporal dementia. *J. Cell Biol.* **208**, 931-947.

Zallen, J. A., Cohen, Y., Hudson, A. M., Cooley, L., Wieschaus, E. and Schejter, E. D. (2002). SCAR is a primary regulator of Arp2/3-dependent morphological events in Drosophila. *J. Cell Biol.* **156**, 689-701.

Zhao, L., Wang, D., Wang, Q., Rodal, A. A. and Zhang, Y. Q. (2013). Drosophila cyfip regulates synaptic development and endocytosis by suppressing filamentous actin assembly. *PLoS Genet.* **9**, e1003450.

Zou, W., Yadav, S., DeVault, L., Nung Jan, Y. and Sherwood, D. R. (2015). RAB-10-dependent membrane transport is required for dendrite arborization. *PLoS Genet.* **11**, e1005484.